ChemComm

COMMUNICATION

View Article Online
View Journal | View Issue

Cite this: *Chem. Commun.*, 2021, **57**, 12277

Received 17th August 2021,
Accepted 26th October 2021

DOI: 10.1039/d1cc04539c

rsc.li/chemcomm

Open-shell extensions to closed-shell pCCD†

Katharina Boguslawski

The pair coupled cluster doubles (pCCD) ansatz represents an inexpensive but accurate single-reference method to describe multi-reference problems. By construction, pCCD remains, however, applicable to closed-shell systems. For the first time, we present extensions to pCCD that allow us to target open-shell molecules with up to 4 unpaired electrons. Although requiring only modest computational cost, our methods approach chemical accuracy for some challenging cases, while their performance is comparable to more expensive models like DMRG or CCSD(T).

The pair coupled cluster doubles (pCCD) model[1,2] is an inexpensive wave function ansatz to describe strongly-correlated closed-shell molecules. It resembles the CCD model, where the cluster operator is restricted to electron-pair excitations $\hat{T}^{\mathrm{pCCD}}$,

$$|\mathrm{pCCD}\rangle = \mathrm{e}^{\left(\sum_{i}^{n_{\mathrm{occ}}}\sum_{a}^{n_{\mathrm{virt}}} c_i^a \hat{a}^\dagger \hat{\bar{a}}^\dagger \hat{\bar{i}}\hat{i}\right)}|\Phi_0\rangle = \mathrm{e}^{\hat{T}^{\mathrm{pCCD}}}|\Phi_0\rangle. \quad (1)$$

In the above equation, the sum runs over all occupied i and virtual a orbitals, $|\Phi_0\rangle$ is some reference determinant, and $\hat{p}$ ($\hat{p}^\dagger$) are the elementary annihilation (creation) operators for spin-up p and spin-down $\bar{p}$ electrons, while c_i^a are the pCCD cluster amplitudes. The exponential form of the ansatz ensures size-extensivity, while size-consistency is restored by optimizing the molecular orbitals.[1–4] The resulting (symmetry-broken) molecular orbital basis is appropriate to model quantum states with (quasi)degeneracies.[3–12] Thus, potential energy surfaces (PESs) that correctly describe dissociation processes are obtained at mean-field-like cost. One drawback of pCCD is, however, that its standard formulation allows us to model only closed-shell systems with an even number of electrons. In this work, we extend the pCCD ansatz to be applicable to open-shell electronic structures with up to 4 unpaired electrons. Our approach exploits the ionization potential equation-of-motion (IP-EOM)[13,14] formalism, where unpaired electrons are introduced by removing electrons from the occupied orbitals of the pCCD reference function. Note that another possibility to treat open-shell molecules, which we have not pursued here, is to switch from the IP to the electron attachment formalism.

EOM-CC[15–17] uses a linear ansatz to parametrize the k-th state

$$|\Psi_k\rangle = \hat{R}(k)|\mathrm{pCCD}\rangle, \quad (2)$$

where the operator $\hat{R}(k)$ generates the targeted state k from the initial pCCD reference state. The explicit form of the operator $\hat{R}(k)$ determines the EOM flavor, like electron excitation, ionization, electron attachment, or spin flip (*cf.* ESI†). Open-shell species are, for instance, accessible by restricting $\hat{R}(k)$ to target either ionized or electron-attached states with respect to the pCCD reference wave function. In this work, we focus on the former, namely the IP-EOM-pCCD model, to remove electrons from the closed-shell pCCD reference function. In the following, we will drop the (k) dependence of $\hat{R}$ to simplify our notation. The ionization operator $\hat{R}$ is typically divided into different parts based on the number of particle (electron creation) and hole (electron annihilation) operators contained in each component. To target quantum states with one unpaired electron, we can exploit the single IP-EOM formalism, where the operator $\hat{R}$ is composed of 1 hole (h) operators, 2 hole and 1 particle (p) operators, *etc.*,

$$\hat{R}^{\mathrm{IP}} = \sum_i r_i \hat{i} + \frac{1}{2}\sum_{ija} r_{ij}^a \hat{a}^\dagger \hat{j}\hat{i} + \ldots = \hat{R}_{1\mathrm{h}} + \hat{R}_{2\mathrm{h}1\mathrm{p}} + \ldots$$

Thus, the single ionization problem annihilates electrons in the (occupied) levels i and may perform electron excitations from occupied to virtual spin orbitals. Similarly, quantum states with two (or more) unpaired electrons can be optimized using the double (D)IP-EOM model, where $\hat{R}$ contains 2h, 3h1p, *etc.*

Institute of Physics, Faculty of Physics, Astronomy and Informatics, Nicolaus Copernicus University in Toruń, ul. Grudziądzka 5, 87-100 Toruń, Poland. E-mail: k.boguslawski@fizyka.umk.pl

† Electronic supplementary information (ESI) available: Theoretical background on EOM-CC, computational details, CCSD(T) PES of DMP^+, details on the electronic structure of CH_2, NH_2^+, SiH_2, and PH_2^+, relative energies for benzynes, singlet–triplet gaps for CH_2 extrapolated to the basis set limit. See DOI: 10.1039/d1cc04539c

operators,

$$\hat{R}^{\mathrm{DIP}} = \frac{1}{2}\sum_{i} r_{ij}\hat{j}\hat{i} + \frac{1}{6}\sum_{ijka} r^{a}_{ijk}\hat{a}^{\dagger}\hat{k}\hat{j}\hat{i} + \ldots = \hat{R}_{2\mathrm{h}} + \hat{R}_{3\mathrm{h1p}} + \ldots$$

The ionized states are obtained from solving the corresponding EOM equations

$$[\hat{H}_N, \hat{R}]|\mathrm{pCCD}\rangle = \omega\hat{R}|\mathrm{pCCD}\rangle, \tag{3}$$

where $\omega = \Delta E - \Delta E_0$ is the change in energy associated with the (single, double, *etc.*) ionization process with respect to the pCCD ground state, while $\hat{H}_N = \hat{H} - \langle\Phi_0|\hat{H}|\Phi_0\rangle$ is the normal-product form of the Hamiltonian. The total electronic energies of the ionized (open-shell) states are then deduced from the total energy of pCCD E_0 and the ionization energy, $E_k = E_0 + \omega$. Since $\hat{R}$ and $\hat{T}^{\mathrm{pCCD}}$ commute, eqn (3) can be simplified as

$$\hat{\mathscr{H}}_N^{\mathrm{pCCD}}\hat{R}|\Phi_0\rangle = \omega\hat{R}|\Phi_0\rangle, \tag{4}$$

where we introduced the similarity transformed Hamiltonian of pCCD in its normal-product form $\hat{\mathscr{H}}_N^{\mathrm{pCCD}} = \mathrm{e}^{-\hat{T}^{\mathrm{pCCD}}}\hat{H}_N\mathrm{e}^{\hat{T}^{\mathrm{pCCD}}}$. The ionization energies are thus the eigenvalues of a non-Hermitian matrix, which can be iteratively diagonalized to determine the lowest-lying ionized states.

High spin ionization potential. In this work, all open-shell wave functions are obtained by solving the IP-EOM equations for the high-spin amplitudes, while the operator $\hat{R}$ is restricted to include at most 2h1p (IP-EOM) or 3h1p (DIP-EOM) terms, respectively. Since the electronic Hamiltonian does not contain any information on the electron spin (like spin–orbit coupling), we can separately optimize the $S_z = -1/2$ and $S_z = -3/2$ cases and the $S_z = 0$, $S_z = -1$ and $S_z = -2$ cases, respectively. For each open-shell molecule, we employed the same pCCD references function in the corresponding IP-EOM and DIP-EOM calculations. Hence, only one (orbital-optimized) pCCD calculation is performed, while different $\hat{R}$ operators are used to target various S_z cases (*cf.* ESI† for computational details). Specficially, for $S_z = -1/2$, the operator $\hat{R}^{\mathrm{IP}}$ contains the following spin blocks

$$\hat{R}^{S_z=-1/2} = \sum_{i} r_i\hat{i} + \frac{1}{2}\sum_{ija} r^{a}_{ij}\hat{a}^{\dagger}\hat{j}\hat{i} + \sum_{ij\bar{a}} r^{\bar{a}}_{ij}\hat{\bar{a}}^{\dagger}\hat{\bar{j}}\hat{i}. \tag{5}$$

The diagonalization of the matrix representation of the similarity-transformed Hamiltonian $\hat{\mathscr{H}}_N^{\mathrm{pCCD}}$ can be thus performed in a specific configurational subspace spanned by the Slater determinants $|\Phi_i\rangle, |\Phi^{a}_{ij}\rangle, |\Phi^{\bar{a}}_{ij}\rangle$ containing $N-1$ electrons (*cf.* ESI† for a pictorial representation of the projection manifold generated by each $\hat{R}$ operator). For $S_z = -3/2$, the operator $\hat{R}^{\mathrm{IP}}$ has a very simple form as only 2h1p terms result in the proper S_z component,

$$\hat{R}^{S_z=-3/2} = \frac{1}{2}\sum_{ij\bar{a}} r^{\bar{a}}_{ij}\hat{\bar{a}}^{\dagger}\hat{\bar{j}}\hat{i}. \tag{6}$$

The diagonalization problem thus reduces to the configurational subspace spanned by $|\Phi^{\bar{a}}_{ij}\rangle$.

In the high-spin DIP-EOM formalism, the $S_z = -1$ states are obtained by restricting the operator $\hat{R}^{\mathrm{DIP}}$ as

$$\hat{R}^{S_z=-1} = \frac{1}{2}\sum_{ij} r_{ij}\hat{j}\hat{i} + \frac{1}{6}\sum_{ijka} r^{a}_{ijk}\hat{a}^{\dagger}\hat{k}\hat{j}\hat{i} + \frac{1}{2}\sum_{ijk\bar{a}} r^{\bar{a}}_{ijk}\hat{\bar{a}}^{\dagger}\hat{\bar{k}}\hat{j}\hat{i}. \tag{7}$$

The corresponding configurational subspace used in the diagonalization problem is thus spanned by $|\Phi_{ij}\rangle, |\Phi^{a}_{ijk}\rangle, |\Phi^{\bar{a}}_{ijk}\rangle$ for $N-2$ electrons. For the $S_z = -2$ case, $\hat{R}^{\mathrm{DIP}}$ includes only 3h1p terms

$$\hat{R}^{S_z=-2} = \frac{1}{6}\sum_{ijk\bar{a}} r^{\bar{a}}_{ijk}\hat{\bar{a}}^{\dagger}\hat{k}\hat{j}\hat{i}, \tag{8}$$

while the diagonalization is restricted to the $|\Phi^{\bar{a}}_{ijk}\rangle$ configurational subspace.

Note that for $S_z = 0$ states, the operator $\hat{R}^{\mathrm{DIP}}$ is restricted to the following spin blocks

$$\hat{R}^{S_z=0} = \sum_{i\bar{j}} r_{i\bar{j}}\hat{\bar{j}}\hat{i} + \frac{1}{2}\sum_{ij\bar{k}a} r^{a}_{ij\bar{k}}\hat{a}^{\dagger}\hat{\bar{k}}\hat{\bar{j}}\hat{i} + \frac{1}{2}\sum_{ij\bar{k}\bar{a}} r^{\bar{a}}_{ij\bar{k}}\hat{\bar{a}}^{\dagger}\hat{\bar{k}}\hat{\bar{j}}\hat{i}, \tag{9}$$

while the configurational subspace during diagonalization is spanned by $|\Phi_{i\bar{j}}\rangle, |\Phi^{a}_{ij\bar{k}}\rangle, |\Phi^{\bar{a}}_{ij\bar{k}}\rangle$. The working equations for all IP-EOM and DIP-EOM flavors mentioned above can be easily derived using diagrammatic techniques as discussed in, for instance, ref. 18 and 19. Here, we assess the performance of three different IP-EOM-based open-shell extensions for pCCD. We focus on the $S_z = 0, -1/2, -1$ IP-EOM flavors. All new open-shell pCCD extensions are implemented in the PyBEST software package.[20] We should stress that such S_z cases can also be efficiently and reliably treated with spin–flip EOM-CCSD methods.[21]

The PES of *N,N′*-dimethylpiperazine (DMP^+). The DMP^+ cation (see Fig. 1b) is an organic model system with a doublet ground state used to investigate intramolecular charge transfer.[25–27] In DMP^+, the charge can either localize on one of the nitrogen atoms of the six-membered ring or delocalize between these two centers. Recent experimental studies[25,26] suggest that the DMP^+ cation features a delocalized ground state, while the energy difference between the localized and

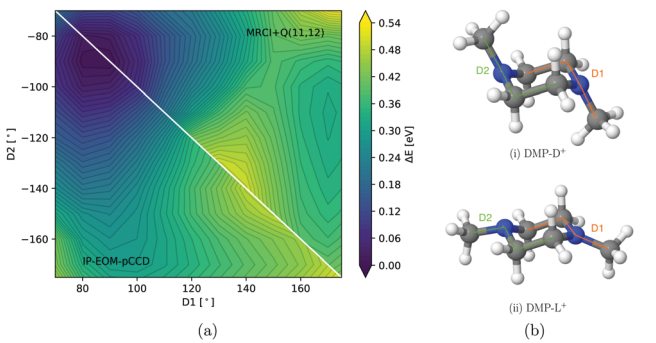

Fig. 1 PESs for (a) IP-EOM-pCCD/aug-cc-pVDZ (bottom) and MRCI+Q(11,12)/cc-pVDZ[22,23] (top) scanned for different dihedral angels D1 and D2 as indicated in (b). For all surfaces, the structures fom ref. 22–24 are used. (b) The relaxed structures of the delocalized ($DMP\text{-}D^+$) and localized ($DMP\text{-}L^+$) state of DMP^+ including both dihedral angles.

delocalized states is anticipated to be small (about 0.33 eV). State-of-the-art wave-function-based methods as well as most density functional approximations fail to predict a local minimum for the localized state, while the errors in the relative energies of the delocalized and localized states are significant.[22,23]

Fig. 1 shows the PES of DMP^+ obtained from IP-EOM-pCCD, which is compared to the corresponding PES of MRCI+Q(11,12) reference calculations[22,23] (for computational details see ESI†). Note that the PES is scanned for two dihedral angles D1 and D2 as illustrated in Fig. 1b. In general, the IP-EOM-pCCD PES is very similar to the one obtained by CCSD(T) (see Fig. S1 of the ESI†) and properly predicts the delocalized state to be the ground state (both dihedral angles are *ca.* 90° in absolute value). Nonetheless, neither CCSD(T) nor IP-EOM-pCCD are able to provide a local minimum for the localized state including the transition state as present in the MRCI+Q(11,12) reference surface.

Table 1 summarizes the energy difference between the localized ($DMP\text{-}L^+$) and delocalized ($DMP\text{-}D^+$) states of DMP^+ obtained by IP-EOM-pCCD and various wave-function-based electronic structure methods. Conventional CASSCF(11,12) calculations do not predict the proper order of states, while second-order N-electron valence perturbation theory on top of various CASSCF reference functions results in large errors with respect to both experiment and MRCI+Q(11,12) data (about 0.4 eV). Conventional single-reference methods like CCSD underestimate $\Delta E_{L,D}$ by about 0.1 eV. IP-EOM-pCCD provides the smallest deviations from experimental and MRCI+Q reference data (<0.05 eV), followed by DMRG-SCF calculations featuring a large active space of 19 electrons correlated in 20 orbitals (*ca.* 0.07 eV).

Methylene and its isovalent analogues. Methylene (CH_2) is a popular test systems to assess the performance of new methods in accurately predicting singlet–triplet gaps.[28,38,39] Here, we will scrutinize adiabatic excitation energies for the lowest-lying states of CH_2 and its isovalent series comprising in addition NH_2^+, SiH_2, and PH_2^+ (see ESI† for more details on their electronic structure).

Table 2 summarizes the adiabatic excitation energies for the three lowest-lying excited states for selected quantum chemistry methods (see also ESI† for complete basis set limit results of CH_2). In general, DIP-EOM-pCCD predicts the proper order of states and character of each excited state. While the lowest-lying singlet–triplet gap is well described by DIP-EOM-pCCD, its performance deteriorates for the higher-lying singlet states. Specifically, the errors with respect to experimental results are small (between 0.02 and 0.04 eV) for the $^3B_1$–$^1A_1$ energy gap and increase to 0.3 eV for the $^1B_1$ and 2^1A_1 state, respectively. Most importantly, the performance of DIP-EOM-pCCD is comparable to more expensive electronic structure methods like SF-OD or CASSCF.

Benzyne isomers. The proper theoretical description of the lowest-lying states of benzynes is a challenge for quantum chemistry due to their diradical nature and multi-reference character, which increase in the sequence *ortho* → *meta* → *para*.[39] Table 3 summarizes the adiabatic singlet–triplet energy splittings for DIP-EOM-pCCD and selected SF, CC, and EOM-CC methods (see also ESI†). In general, DIP-EOM-pCCD predicts the proper order of states, while the singlet–triplet gaps differ by 0.06–0.2 eV from experimental values. The smallest errors are obtained for *meta*- and *para*-benzyne (0.06 eV), whose electronic structures feature strong multi-reference character, while the errors increase to approximately 0.2 eV for *ortho*-benzyne. Most importantly, DIP-EOM-pCCD outperforms the conventional (and computationally more expensive) CCSD

Table 1 Energy differences [eV] between $DMP\text{-}L^+$ and $DMP\text{-}D^+$ calculated using the same structures[22–24] for different quantum chemistry methods and the aug-cc-pVDZ basis set. $\Delta E_{L,D} = E(DMP - L^+) - E(DMP - D^+)$. $\Delta\Delta E$ is the deviation of the energy difference from experiment or MRCI reference data

Method	$\Delta E_{L,D}$	$\Delta\Delta E$ (exp)	$\Delta\Delta E$ (MRCI)
IP-EOM-pCCD	0.378	0.048	0.042
CCSD[22]	0.222	−0.108	−0.114
CASSCF(11,12)[22]	−0.017	−0.347	−0.353
DMRG-SCF(19,20)[22]	0.266	−0.064	−0.070
NEVPT2(11,12)[22]	0.771	0.441	0.435
FIC-MRCI+Q(11,12)[22]	0.336	0.006	0.000
Experiment[25]	0.330	0.000	−0.006

Table 2 Total energies [E_h] for the ground state of CH_2, NH_2^+, SiH_2, and PH_2^+ and adiabatic excitation energies [eV] for the three lowest-lying excited states obtained by different electronic structure methods. In all DIP-EOM-pCCD calculations, the cc-pVTZ basis set was used. For all SF, CC, and EOM-CC methods, a TZ2P basis set was employed for CH_2, while a TZ2P(f,d) basis set was used for NH_2^+, SiH_2, and PH_2^+

	$^3B_1$	$^1A_1$	$^1B_1$	2^1A_1
CH_2				
DIP-EOM-pCCD	−39.01391	0.413	1.726	2.799
CCSD[28]	−39.08092	0.545	—	2.054
CCSD(T)[28]	−39.08386	0.505	—	1.907
EOM-CCSD[28]	−39.08066	0.538	1.566	3.843
SF-CCSD[29]	−39.08046	0.517	1.565	2.718
SF-CCSD(fT)[29]	−39.08184	0.500	1.552	2.688
Experiment[30]		0.390	1.425	
NH_2^+				
DIP-EOM-pCCD	−55.31909	1.350	2.226	3.489
SF-CIS[28]	−55.22731	1.673	2.151	4.375
SF-OD[28]	−55.40259	1.305	1.941	3.419
CASSCF SOCI[31]	−55.388368	1.281	1.935	3.380
Experiment[32]		1.306 ± 0.01		
	$^1A_1$	$^3B_1$	$^1B_1$	2^1A_1
SiH_2				
DIP-EOM-pCCD	−290.12645	0.935	2.256	3.883
SF-CIS[28]	−290.03701	0.503	2.199	3.945
SF-OD[28]	−290.29961	0.866	1.994	3.537
CASSCF SOCI[33]	−290.166351	0.871	1.992	3.486
Experiment		0.91 ± 0.03[34]	1.928[35]	
PH_2^+				
DIP-EOM-pCCD	−341.64276	0.775	2.254	3.941
SF-CIS[28]	−341.55130	0.388	2.166	4.541
SF-OD[28]	−341.74916	0.761	2.015	3.728
CASSCF SOCI[36]	−341.695054	0.760	2.009	3.686
Experiment[37]		0.75 ± 0.05	1.92	

Table 3 Adiabatic excitation energy [eV] to the lowest-lying triplet state of *ortho*-, *meta*, and *para*-benzyne using the cc-pVTZ basis set

	ortho-Benzyne	*meta*-Benzyne	*para*-Benzyne
DIP-EOM-pCCD	1.398	0.856	0.221
DIP-EOM-CCSD[39]	1.847	0.854	0.191
DEA-EOM-CCSD[40]	1.625	0.799	0.145
CCSD[39]	1.327	0.455	−0.833
CCSD(T)[39]	1.604	0.958	0.156
SF-CCSD[29]	1.578	0.782	0.147
SF-CCSD(fT)[29]	1.615	0.875	0.169
Experiment[41]	1.628 ± 0.013	0.911 ± 0.014	0.165 ± 0.016

method and provides similar errors in singlet–triplet gaps as the DIP-EOM-CCSD approach.

To sum up, the errors of (D)IP-EOM-pCCD in (relative) electronic energies are small and lie between 0.02 eV (0.46 kcal mol^{-1}) and 0.2 eV (4.6 kcal mol^{-1}). For the most challenging cases like DMP^+ and *meta*- or *para*-benzyne, (D)IP-EOM-pCCD approaches chemical accuracy (approximately 0.04 eV or 1 kcal mol^{-1}) and its performance is comparable to more expensive single- or multi-reference methods like DMRG, CCSD(T), or DIP-EOM-CCSD. To conclude, the high-spin IP- and DIP-EOM-pCCD model represent a simple alternative to target open-shell states starting from the closed-shell pCCD reference function. Finally, their performance can be further improved by including dynamical correlation on top of the pCCD reference function, for instance using the fpCC[42] formalism or its linearized variant.[9,43] The resulting fpCC and fpLCC wave functions can be straightforwardly combined with an IP- or DIP-EOM treatment. A deeper analysis of the performance and potential drawbacks of the (D)IP ansatz[44] (*e.g.* robustness of the +2 reference state, pCCD orbitals, *etc.*) will be the subject of a forthcoming publication.

We acknowledge financial support from the National Science Centre, Poland (No. 2015/18/E/ST4/00584). Calculations have been carried out using resources provided by Wroclaw Centre for Networking and Supercomputing (http://wcss.pl), Grant No. 412. We thank Marta Gałyńska for providing us the structures of DMP^+ and the CCSD(T) and MRCI+Q reference PESs.

Conflicts of interest

There are no conflicts to declare.

Notes and references

1 K. Boguslawski, P. Tecmer, P. W. Ayers, P. Bultinck, S. De Baerdemacker and D. Van Neck, *Phys. Rev. B: Condens. Matter Mater. Phys.*, 2014, **89**, 201106(R).
2 T. Stein, T. M. Henderson and G. E. Scuseria, *J. Chem. Phys.*, 2014, **140**, 214113.
3 K. Boguslawski, P. Tecmer, P. A. Limacher, P. A. Johnson, P. W. Ayers, P. Bultinck, S. De Baerdemacker and D. Van Neck, *J. Chem. Phys.*, 2014, **140**, 214114.
4 K. Boguslawski, P. Tecmer, P. W. Ayers, P. Bultinck, S. De Baerdemacker and D. Van Neck, *J. Chem. Theory Comput.*, 2014, **10**, 4873–4882.
5 P. Tecmer, K. Boguslawski and P. W. Ayers, *Phys. Chem. Chem. Phys.*, 2015, **17**, 14427–14436.
6 A. J. Garza, A. G. S. Alencar and G. E. Scuseria, *J. Chem. Phys.*, 2015, **143**, 244106.
7 A. J. Garza, I. W. Bulik, T. M. Henderson and G. E. Scuseria, *Phys. Chem. Chem. Phys.*, 2015, **17**, 22412–22422.
8 K. Boguslawski, *J. Chem. Phys.*, 2016, **145**, 234105.
9 K. Boguslawski and P. Tecmer, *J. Chem. Theory Comput.*, 2017, **13**, 5966–5983.
10 K. Boguslawski, *J. Chem. Theory Comput.*, 2019, **15**, 18–24.
11 A. Nowak, P. Tecmer and K. Boguslawski, *Phys. Chem. Chem. Phys.*, 2019, **21**, 19039–19053.
12 P. Tecmer, K. Boguslawski, M. Borkowski, P. S. Żuchowski and D. Kedziera, *Int. J. Quantum Chem.*, 2019, **119**, e25983.
13 M. Nooijen and J. G. Snijders, *Int. J. Quantum Chem.*, 1992, **44**, 55–83.
14 M. Nooijen and J. G. Snijders, *Int. J. Quantum Chem.*, 1993, **48**, 15–48.
15 A. I. Krylov, *Annu. Rev. Phys. Chem.*, 2008, **59**, 433–462.
16 K. Sneskov and O. Christiansen, *Wiley Interdiscip. Rev.: Comput. Mol. Sci.*, 2012, 566–584.
17 R. J. Bartlett, *Wiley Interdiscip. Rev.: Comput. Mol. Sci.*, 2012, **2**, 126–138.
18 M. Musiał, S. A. Kucharski and R. J. Bartlett, *J. Chem. Phys.*, 2003, **118**, 1128–1136.
19 M. Musiał, L. Lupa and S. A. Kucharski, *J. Chem. Phys.*, 2014, **140**, 114107.
20 K. Boguslawski, A. Leszczyk, A. Nowak, F. Brzek, P. S. Żuchowski, D. Kedziera and P. Tecmer, *Comput. Phys. Commun.*, 2021, **264**, 107933.
21 D. Casanova and A. I. Krylov, *Phys. Chem. Chem. Phys.*, 2020, **22**, 4326–4342.
22 M. Gałyńska, V. Ásgeirsson, H. Jónsson and R. Björnsson, 2020, arXiv:2007.06125 [physics.chem-ph].
23 M. Gałyńska, V. Ásgeirsson, H. Jónsson and R. Björnsson, *J. Phys. Chem. Lett.*, 2021, **12**, 1250–1255.
24 The DMP^+ structures were provided by Marta Gałyńska.
25 S. Deb, X. Cheng and P. M. Weber, *J. Phys. Chem. Lett.*, 2013, **4**, 2780–2784.
26 X. Cheng, Y. Zhang, E. Jónsson, H. Jónsson and P. M. Weber, *Nat. Commun.*, 2016, **7**, 11013.
27 Z. A. Ali, F. W. Aquino and B. M. Wong, *Nat. Commun.*, 2018, **9**, 4733.
28 L. V. Slipchenko and A. I. Krylov, *J. Chem. Phys.*, 2002, **117**, 4694.
29 P. U. Manohar and A. I. Krylov, *J. Chem. Phys.*, 2008, **129**, 194105.
30 P. Jensen and P. R. Bunker, *J. Chem. Phys.*, 1988, **89**, 1327–1332.
31 J. C. Stephens, Y. Yamaguchi, C. D. Sherrill and H. F. Schaefer III, *J. Phys. Chem. A*, 1998, **102**, 3999–4006.
32 S. T. Gibson, J. P. Greene and J. Berkowitz, *J. Chem. Phys.*, 1985, **83**, 4319–4328.
33 Y. Yamaguchi, T. J. Van Huis, C. D. Sherrill and H. F. Schaefer III, *Theor. Chem. Acc.*, 1997, **97**, 341–349.
34 J. Berkowitz, J. P. Greene, H. Cho and B. Ruščić, *J. Chem. Phys.*, 1987, **86**, 1235–1248.
35 R. Escribano and A. Campargue, *J. Chem. Phys.*, 1998, **108**, 6249–6257.
36 T. J. Van Huis, Y. Yamaguchi, C. D. Sherrill and H. F. Schaefer, *J. Phys. Chem. A*, 1997, **101**, 6955–6963.
37 J. Berkowitz and H. Cho, *J. Chem. Phys.*, 1989, **90**, 1–6.
38 X. Li and J. Paldus, *J. Chem. Phys.*, 2008, **129**, 174101.
39 A. Perera, R. W. Molt Jr., V. F. Lotrich and R. J. Bartlett, *Theor. Chem. Acc.*, 2014, **133**, 1514.
40 S. Gulania, E. F. Kjønstad, J. F. Stanton, H. Koch and A. I. Krylov, *J. Chem. Phys.*, 2021, **154**, 114115.
41 P. G. Wenthold, R. R. Squires and W. C. Lineberger, *J. Am. Chem. Soc.*, 1998, **120**, 5279–5290.
42 T. M. Henderson, I. W. Bulik, T. Stein and G. E. Scuseria, *J. Chem. Phys.*, 2014, **141**, 244104.
43 K. Boguslawski and P. W. Ayers, *J. Chem. Theory Comput.*, 2015, **11**, 5252–5261.
44 T. Kuś and A. I. Krylov, *J. Chem. Phys.*, 2011, **135**, 084109.

